Geophysical Research Letters

RESEARCH LETTER
10.1029/2020GL087593

Formation and Evolution of the Large-Scale Magnetic Fields in Venus' Ionosphere: Results From a Three Dimensional Global Multispecies MHD Model

Yingjuan Ma[1], Gabor Toth[2], Andrew Nagy[2], Janet Luhmann[3], and Christopher Russell[1]

[1]Department of Earth, Planetary, and Space Sciences, University of California Los Angeles, Los Angeles, CA, USA, [2]Department of Climate and Space Sciences and Engineering, University of Michigan, Ann Arbor, MI, USA, [3]Space Sciences Laboratory, University of California, Berkeley, CA, USA

Key Points:
- The global MHD model self-consistently reproduces the formation and evolution of the large-scale magnetic fields in the Venus ionosphere
- Model results show that it takes quite long time (~hr) for the magnetic field to penetrate into and decay in the ionosphere
- The large-scale magnetic fields in the ionosphere act as an additional obstacle to the solar wind

Supporting Information:
- Supporting Information S1

Correspondence to:
Y. Ma,
yingjuan@igpp.ucla.edu

Citation:
Ma, Y., Toth, G., Nagy, A., Luhmann, J., & Russell, C. (2020). Formation and evolution of the large-scale magnetic fields in Venus' ionosphere: Results from a three dimensional global multispecies MHD model. *Geophysical Research Letters*, *47*, e2020GL087593. https://doi.org/10.1029/2020GL087593

Received 19 FEB 2020
Accepted 22 APR 2020
Accepted article online 10 MAY 2020

Abstract Large-scale magnetic fields have been observed in Venus' ionosphere by both the Pioneer Venus Orbiter (PVO) and Venus Express spacecraft. In this study, we examine the formation and evolution of the large-scale magnetic field in the Venus ionosphere using a sophisticated global multispecies Magnetohydrodynamics (MHD) model that has been developed for Venus (Ma et al., 2013, https://doi.org/10.1029/2012JA018265). A time-dependent model run is performed under varying solar wind dynamic pressure. Based on model results, we find that (1) the initial response of the induced magnetosphere is fast (~min), (2) a large-scale magnetic field gradually forms in the ionosphere when the solar wind dynamic pressure suddenly exceeds the ionospheric thermal pressure, (3) both the penetration and decay of the large-scale magnetic field in the ionosphere are slow (~hr), and (4) the ion escape rate has a nonlinear response to the change of solar wind dynamic pressure.

Plain language Summary Large-scale magnetic fields have been observed at Venus' ionosphere by previous Venus missions. In this study, we examine the formation and evolution of the large-scale magnetic field in the Venus ionosphere using a sophisticated global model. A time-dependent model run is performed under varying solar wind dynamic pressure (density). Model results show that the outside interaction region responds quickly (~min) to the solar wind variation, while the response time of the ionosphere is long (~hr). We also found that the ion escape rate has a nonlinear response to the change of solar wind dynamic pressure.

1. Introduction

Pioneer Venus Orbiter (PVO) observations have shown clear evidence that Venus has no significant global intrinsic field (Phillips & Russell, 1987). As a result, its atmosphere and ionosphere interact with the solar wind much more directly, in contrast to Earth (Cravens, 1989; Futaana et al., 2017). PVO observations have also shown that Venus' ionosphere has two distinct states: magnetized and unmagnetized, commonly thought to be controlled by the relative strength of the solar wind dynamic pressure and ionosphere thermal pressure (Cravens, 1989). During solar maximum conditions, the ionospheric thermal pressure is normally stronger than the solar wind dynamic pressure, and the ionosphere is often found to be in the unmagnetized state, due to the high electrically conducting property of the ionosphere, which enables a strong current to fully stop the penetration of the induced magnetic field. During solar minimum conditions, the solar wind dynamic pressure is normally larger than the ionospheric thermal pressure. Thus, the induced magnetic field could at least partially penetrate into the ionosphere, resulting in a magnetized ionosphere. Such a scenario was first confirmed using self-consistent global MHD models by Ma et al. (2013), under steady-state solar wind conditions. As both the upstream solar wind conditions and solar extreme ultraviolet (EUV) flux constantly vary with time, the relative strength of the solar wind dynamic pressure and the ionospheric thermal pressure could also vary. Thus, the state of the ionosphere is expected to change from one to the other in response to variations of external drivers, especially solar wind dynamic pressure. A clear example of such change is shown by PVO observations for three consecutive orbits: 175, 176, and 177 (Elphic et al., 1980). However, how the ionosphere changes from one state to another has not been fully understood, due to limitations of single spacecraft observations.

The magnetic field profiles in the magnetized ionosphere are far from uniform. A large-scale magnetic field (sometimes called low-altitude magnetic belt) was found in the dayside ionosphere in both PVO and Venus Express (VEX) observations (Luhmann et al., 1980; Russell et al., 1983; Villarreal et al., 2015). These large-scale fields are mainly horizontal and usually show a distinct minimum near ~200 km altitude (Luhmann et al., 1980). Russell et al. (1983) first suggested that time variations are essential to explaining the observed features of the low-altitude magnetic belt, as the observations of the large-scale magnetic field likely occurred sometime after it had been created and evolved. The evolution of large-scale fields has been studied by Cloutier (1984), and Cravens et al. (1984), Luhmann et al. (1984), using various one-dimensional approaches, solving mainly the magnetic diffusion equation. The estimated decay time scale ranges from 2–3 min (Cloutier, 1984) to 10 min to a few hours, depending on assumptions on vertical velocities (Cravens et al., 1984). Later, more comprehensive 1D and 2D multispecies MHD models were developed for Venus by Shinagawa and coauthors (Shinagawa, 1996a, 1996b; Shinagawa et al., 1987, 1991; Shinagawa & Cravens, 1988), which were able to reproduce many observed features below 250 km altitude, including the electron density "ledge" near 190 km altitude and a decrease of magnetic field around 200 km altitude. However, significant disagreement between the calculated and observed plasma densities at high altitudes suggested that a 3D global model is needed to understand the formation and the evolution of the large-scale magnetic fields in the Venus ionosphere, due to the three-dimensional nature of the solar wind interaction with the Venus ionosphere.

In addition, previous statistical studies have found a positive correlation between ion escape rates and upstream solar wind dynamic pressure (Edberg et al., 2011; Luhmann et al., 2007). However, there is little understanding of the ionospheric responses to solar wind variations, due to the lack of coordinated observations of both upstream solar wind conditions and simultaneous plasma properties in the Venus ionosphere. In this paper, we use a sophisticated multispecies MHD model developed for Venus (Ma et al., 2013), to characterize the changes of the ionosphere and the induced magnetosphere (IM) under varying solar wind dynamic pressure. This model enables us to answer the question of how the ionosphere changes from one state to another. We briefly describe the model used for the study in section 2. The model results are present in section 3, followed by discussion and summary in section 4.

2. Time-Dependent Global Multi-Species MHD Model

The multispecies global MHD model of Venus based on the BATS-R-US code (Tóth et al., 2012) is described in detail in Ma et al. (2013). Model results of three cases are presented in Ma et al. (2013), corresponding to solar max, solar min, and a VEX case, which are in good agreement with the observations of both PVO and VEX in terms of both bow shock locations and magnetic field observations. The model solves continuity equations of multiple ion species for H^+, O^+, O_2^+, and CO_2^+, and momentum and energy, and magnetic field induction equations. The simulation uses the Venus Solar Orbital (VSO) coordinates, with a computational domain of $-24\ R_V \le X \le 8\ R_V$, $-16\ R_V \le Y$, and $Z \le 16\ R_V$, where $R_V = 6{,}052$ km is the radius of Venus. The inner boundary was taken to be 100 km above the Venus surface in a collision-dominated region, and thus, we assume ion densities are in photochemical equilibrium. The inner boundary conditions for U and B are the same as described in Ma et al. (2013), assuming zero gradients for both vectors. The angular resolution is kept at 2.5°, both azimuthally and longitudinally in the computation domain. The radial resolution is 5 km (~0.0008 R_V) from the lower boundary (100 km) to 500 km altitude; above this altitude, the radial resolution gradually increases from 5 to 2,000 km (0.34 R_V) near the outer boundary at 24 R_V downstream. Such a grid contains 480 × 144 × 72 (about 5 million) cells in total. Ionospheric conductivity is included in the model and is calculated in the same way as described in Ma et al. (2013).

To understand the formation and evolution of the large-scale magnetic field in the Venus ionosphere, we run an idealized solar wind dynamic pressure enhancement event with time-varying solar wind conditions. In the event, the dynamic pressure enhancement is realized by changing only the solar wind density, with all the other input parameters unchanged. We first run the model under quiet solar wind conditions for 1 hr to reach a quasi-steady state and then enhance the solar wind density by a factor of 2, which lasts for 2 hr, as shown in Figure 1a. The density then returns to quiet conditions for 2 hr, with a total simulation time of 5 hr. The quiet solar wind condition is taken to be the same as in case 1 (solarmax case) of Ma et al. (2013), with $n_{SW} = 17\ cm^{-3}$; U = −400 km/s, B_{IMF} = (12.1, −8.8, 0) nT, and $T_{SW} = 2.5 \times 10^5$ K. The corresponding

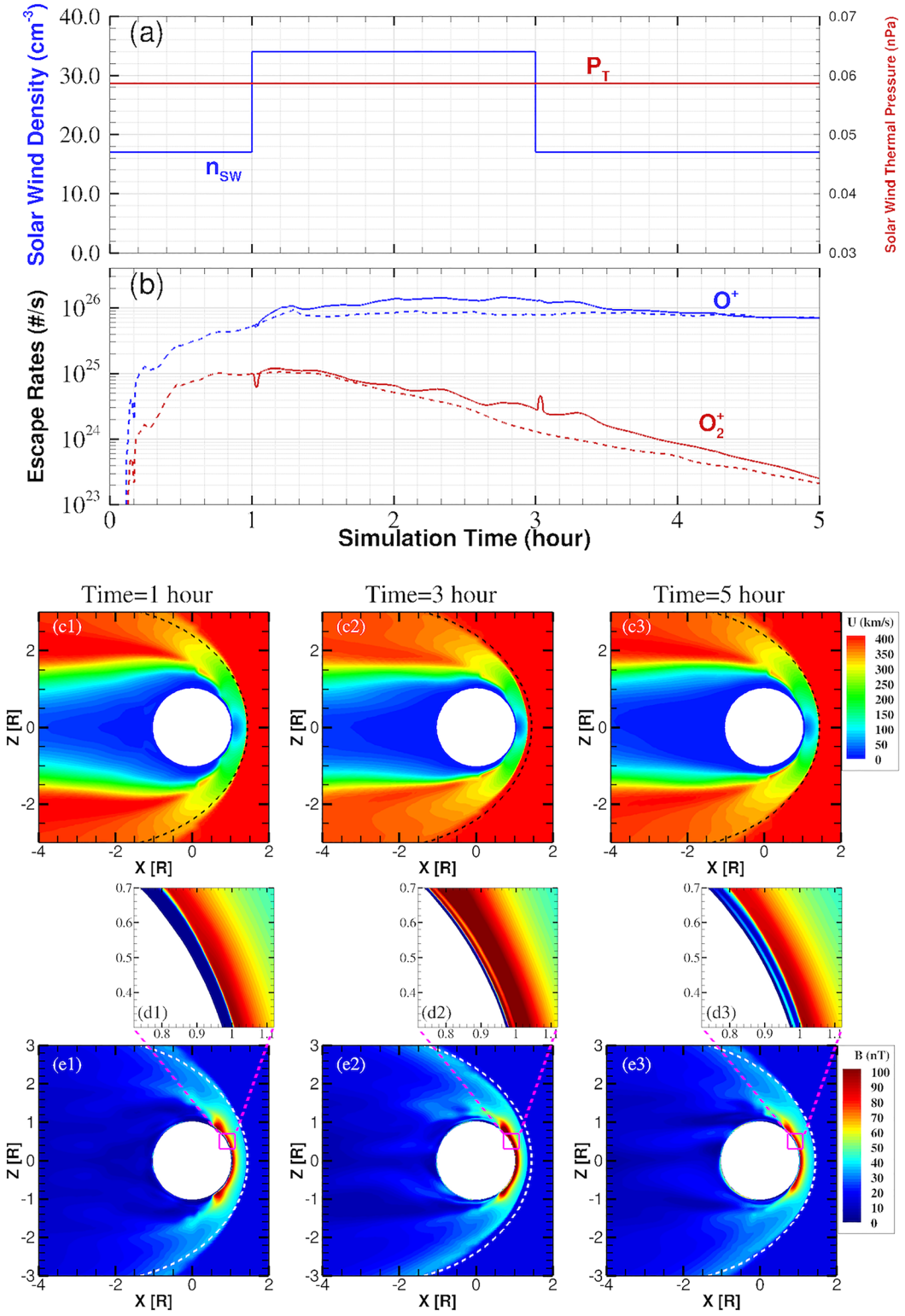

FIGURE 1. (a) Solar wind density and thermal pressure profiles used in the simulation. (b) Ion escape rates during the high-pressure pulse event (solid lines). The escape rates using quiet solar wind conditions are shown in dashed lines for reference. Contour plots of (c1–c3) show plasma flow speed and (e1–e3) magnetic field strength in the *XZ* plane at 1, 3, and 5 hr, respectively. The dashed white curves show the average bow shock locations at solar maximum condition from Zhang et al. (1990). Zoom-in views of the magnetic field strength inside the purple region of 0.72 $R_V < X < 1.12$ R_V and 0.3 $R_V < Z < 0.7$ R_V are shown in panels d1–d3.

solar wind dynamic pressure is 4.5 nPa, and the fast magnetosonic Mach number is 4.2. The neutral density and EUV flux are also set for solar maximum conditions. The disturbed solar wind propagates into the simulation domain from the upstream outer boundary at $X = -8$ R_V. This is an idealized event of a dynamic pressure pulse. In reality, the density, velocity, and magnetic field could all vary. However, it could be challenging to distinguish causes and consequences, as the impacts of these parameters are mixed. In this sense, simple events are more useful in probing the physical processes in the Venus-solar wind interaction. The simulation results of the event are presented in the next section.

3. Model Results

The variation of the ion escape rates during this ideal solar wind density pulse event is calculated through integrating the net ion fluxes through the 5 R_V sphere and is shown in Figure 1b (solid lines). For solar maximum conditions, the O^+ ion is by far the most dominant ion escaping from Venus. Note that the CO_2^+ escape flux is about 5 orders smaller than O^+, less than 1×10^{21} (not shown in the figures). To highlight the changes of escape rates due to varying solar wind conditions, we also plot the escape rates in dashed lines for the baseline case, using constant solar wind conditions for reference. The total ion escape rate for quiet solar wind conditions averaged over 4 hr (1–5 hr) is around 8×10^{25} particles/s, and the corresponding mass loss is ~2.14 kg/s. During the 2-hour period of high solar wind dynamic pressure, the O^+ escape rate increased about 49.6% on average. The ion escape rates are still significantly high, especially for the first 30 min after the density pulse. The O^+ loss rate is still 27% higher on average for the first hour (between 3 and 4 hr). The ion escape rates produced by the model for solar maximum under quiet solar wind conditions is consistent with the value estimated by Brace et al. (1987), 5×10^{25} particles/s, but much larger than the ~1×10^{25} particles/s estimated by McComas et al. (1986), both using PVO observations. The escape rates are also much larger than 2.7×10^{24} particles/s, estimated for solar minimum conditions using VEX observations (Fedorov et al., 2011). The large enhancement of the ion escape rate at times of high solar wind dynamic pressure is consistent with findings of Luhmann et al. (2007).

The rest of the panels in Figure 1 illustrate how the interaction changes globally during the density pulse event. Panels c1–c3 show plasma velocity distribution in the *XZ* plane at 1, 3, and 5 hr, corresponding to quiet time, under enhanced solar wind density and 2 hr after the solar wind returned to quiet conditions, respectively. The bow shock locations from the model at quiet solar wind conditions, both at 1 and 5 hr, match very well with the mean bow shock locations for solar maximum (Zhang et al., 1990), except that they are closer to the planet near the subsolar region and farther away near the flank regions. This is because the bow shock fitting function assumed that the bow shock locations are axial symmetric, while in reality, the bow shock locations are asymmetric in the terminator plane, farther away from the planet in the direction perpendicular to the magnetic field (in the *Z* direction), compared with the parallel direction (*Y* direction), as observed by PVO (Russell et al., 1988). At 3 hr, when the solar wind dynamic pressure is high, the bow shock locations are significantly compressed. The bottom panels show corresponding magnetic field strength contour plots. There is a clear magnetic field enhancement (IM) near the planet. Also, the peak magnetic field is the highest at 3 hr, as expected. To show clearly the different magnetic state of the ionosphere, we also show zoom-in views of the magnetic field strength inside the region of $0.72\ R_V < X < 1.12$ Rv and $0.3\ R_V < Z < 0.7\ R_V$ (panels d1–d3). As can be clearly seen, the ionosphere is in the unmagnetized state at 1 hr, strongly magnetized state at 3 hr, and there is a low-altitude magnetic belt in the ionosphere at 5 hr. The peak magnetic fields are 115, 98, 34, and 27 nT at 0, 30, 60, and 90 SZA, respectively at 3 hr (see Figure S1 in the supporting information). The magnetic fields in the low-altitude belt are weaker at large SZA, consistent with PVO observations (Luhmann et al., 1980).

To examine in more detail how the Venus space environment responds to the density (pressure) pulse event, we also plotted the snapshots of various pressure profiles along the subsolar line for different times, as shown in Figure 2. In each panel, pressure profiles of thermal pressure (in blue), dynamic pressure (in red), magnetic pressure (green), and total pressure (black) are plotted. Before the pressure pulse reaches Venus, solar wind dynamic pressure (~4.5 nPa) is smaller than the peak of the ionospheric thermal pressure (~8.2 nPa), and the Venus ionosphere is unmagnetized and dominated by thermal pressure (see panel a). It takes about 1 min and 40 s for the pressure pulse to propagate from the outer boundary to the Venus bow shock locations (see panel b), and the solar wind dynamic pressure doubles outside of the bow shock due to enhancement of

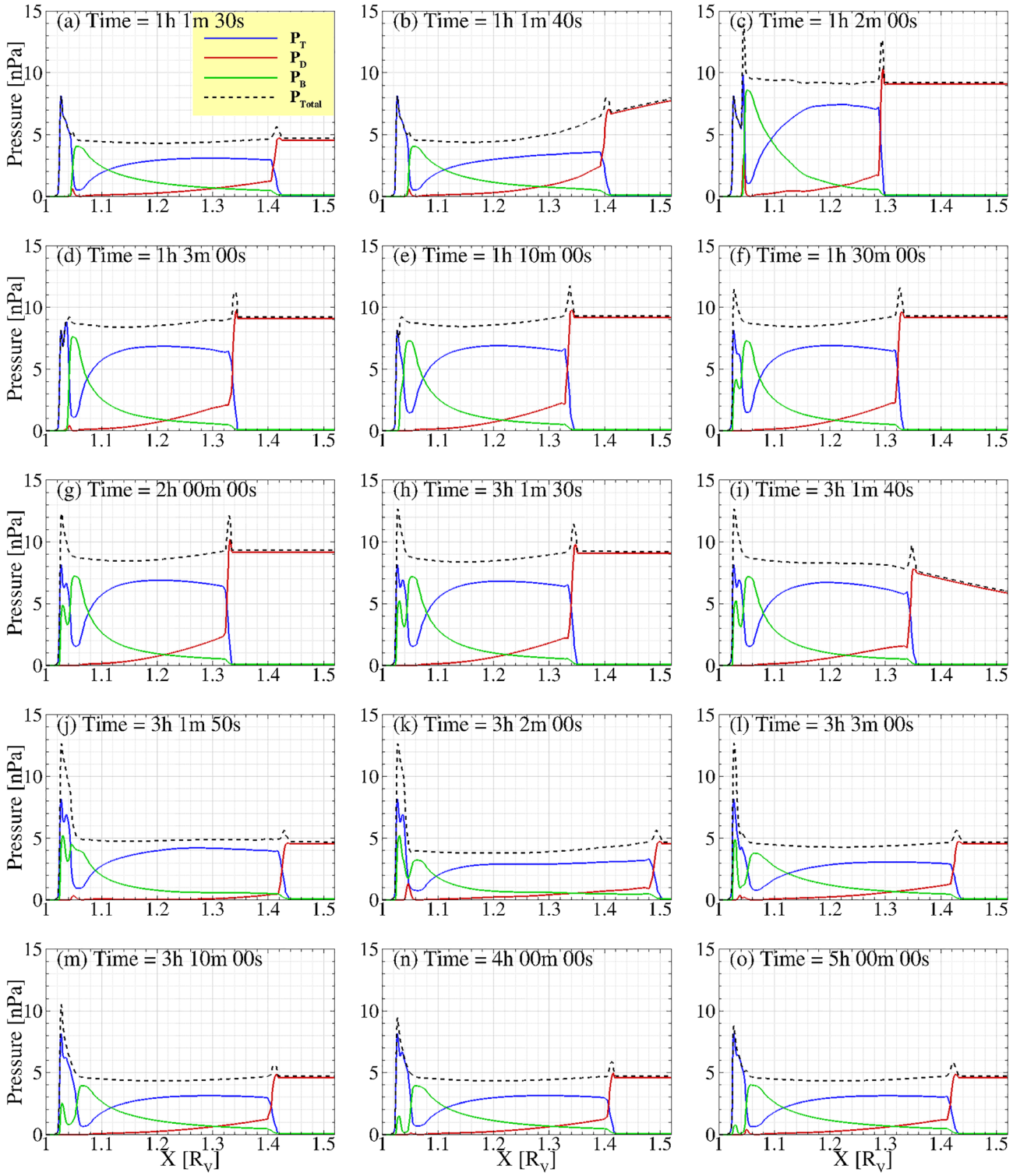

FIGURE 2. Snapshots of pressure profiles along the subsolar line during the solar wind density pulse event. Pressure profiles of thermal pressure (in blue), dynamic pressure (in red), magnetic pressure (green), and total pressure (black) are plotted in each panel.

the solar wind density. The high solar wind dynamic pressure pushes the bow shock location from 1.4 R_V inward all the way to 1.3 R_V, in less than 20 s (see panel c). Across the shock, the solar wind dynamic pressure is converted mostly to thermal pressure in the sheath region, so the thermal pressure inside the

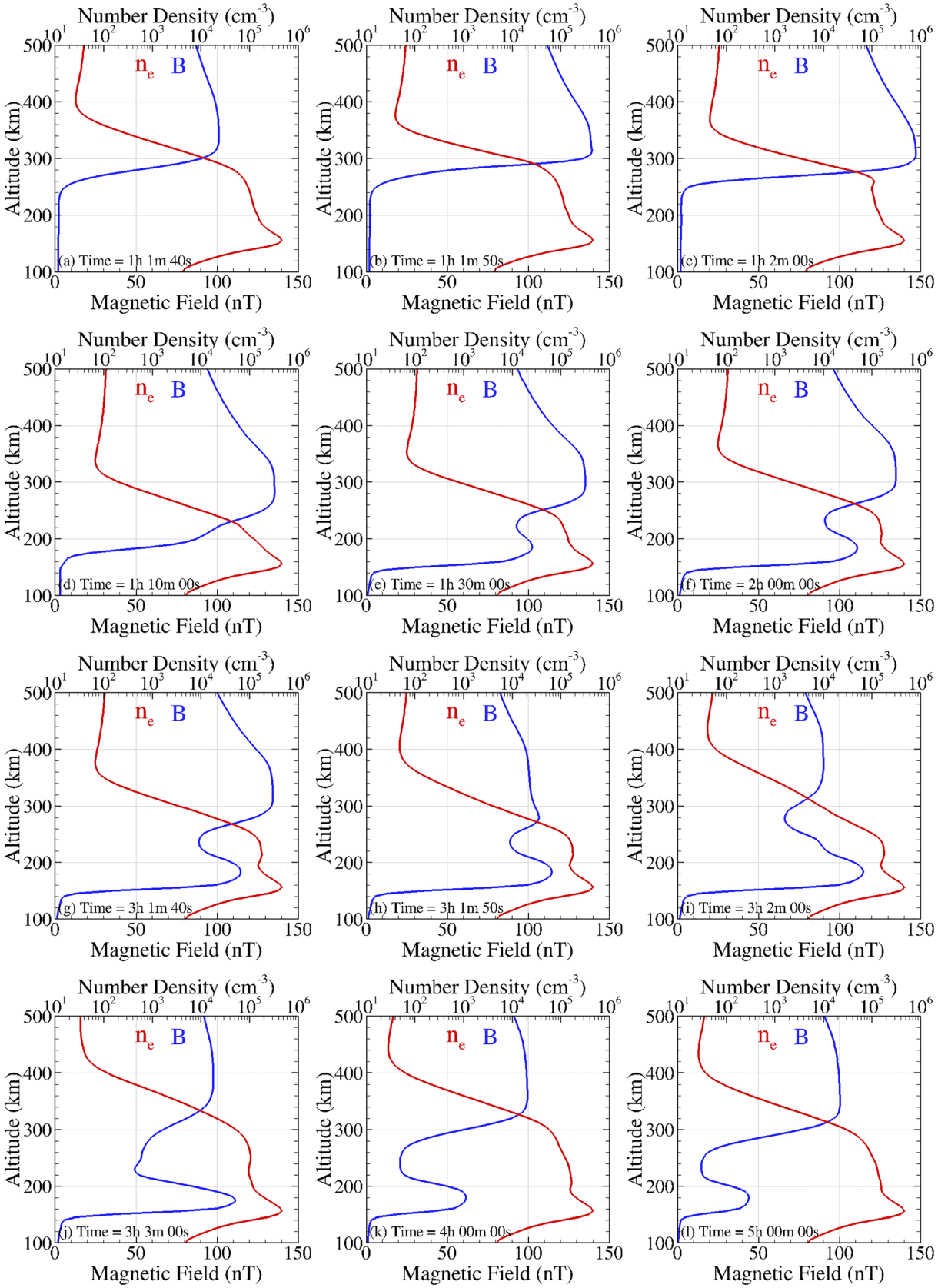

FIGURE 3. Density and magnetic field responses to solar wind density variations along the subsolar line.

shock increases nearly by a factor of two, shortly after the pressure pulse arrival. Closer to the planet, the peak magnetic pressure also doubles in the IM. Both the magnetosheath region and IM respond quickly to the enhanced solar wind dynamic pressure in 10s of seconds. The predicted timescale is similar to the recovery timescale of the Martian magnetosphere to interplanetary magnetic field (IMF) variations as estimated by a hybrid model (Romanelli et al., 2019). The bow shock locations bounce back a little and settle at around 1.33 R_V along the subsolar point (see panel d). Even though the solar wind dynamic pressure is higher than the ionospheric peak pressure, the magnetic field does not penetrate into the ionosphere right away. In fact, simulation results show that the penetration of the magnetic field into the ionosphere is a much slower process, taking nearly an hour to form a magnetized ionosphere (panels e and f). The magnetic field gradually increases at lower altitude, forming a local maximum near the ionospheric thermal pressure peak and a local minimum above. At the end of the pressure pulse, around 3 hr (see panel h), the peak magnetic pressure in the ionosphere is about 60% of the peak value in the IM region.

When the pressure pulse ends at the outer boundary and propagates to Venus around 03:01:40 (panel i), the dynamic pressure outside the bow shock drops back to 4.5 nPa, and the bow shock location quickly moves outward from 1.32 to 1.5 R_V (panels j and k). The peak magnetic pressure in the IM and the thermal pressure in the mangetosheath region adjust rapidly back to the new solar wind conditions. However, the magnetic field inside the ionosphere responds much more slowly to the solar wind dynamic pressure variation. The magnetic field inside the ionosphere slowly diffuses away (panels m and n). The fields inside the ionosphere are largely horizontal "fossil fields," existing more than 2 hr after the density pulse event (panel o).

The variations of electron number density and magnetic field in the ionosphere are shown in Figure 3 to further help us understand the ionospheric responses. Panels a–g illustrate how the magnetic field gradually penetrates into the ionosphere during high solar wind pressure enhancement. It takes about 10 more seconds (panels b and c) for the magnetic field to be enhanced above the ionosphere. The peak magnetic field reaches around 150 nT at 1 hr and 2 min, while the field inside the ionosphere is still nearly zero. The large pressure gradient force pushes the plasma downward, with downward convecting magnetic field flux. Because of the large ion-neutral collision frequency, the flow speed inside the ionosphere is extremely low (in the order of m/s), so the convection of the magnetic field flux is a slow process (panels d–g). Panels h–l show the electron number density and magnetic field strength variations along the subsolar line after the pressure pulse, as the fossil magnetic field in the ionosphere gradually diffuses away. It is important to note that as the magnetic field penetrates into the ionosphere, the density profiles were also significantly altered. We also checked the variation of the ion composition during the event and found that below 250 km altitude, the ion composition is quite steady.

The evolution of the magnetic field in the ionosphere can be understood with the help of the magnetic induction equation

$$\frac{\partial B}{\partial t}=\nabla\times(u\times B)-\nabla\times(\eta_m\nabla\times B), \tag{1}$$

where η_m is magnetic diffusivity. Based on equation 1, the change of magnetic field depends on two terms on the right side of the equation, corresponding to convection and diffusion/dissipation, respectively. As the magnetic field is mainly the horizontal component B_Y, along the subsolar line, equation 1 can be simplified as

$$\frac{\partial B_Y}{\partial t}=\frac{\partial}{\partial x}(V_x B_Y)+\frac{\partial}{\partial x}\left(\eta_m\frac{\partial}{\partial x}B_Y\right). \tag{2}$$

Panels 1b, 2b, and 3b in Figure 4 show the vertical plasma flow (U_X) and magnetic resistivity (η_m) at 1, 3, and 5 hr (solid lines), respectively. At high altitude, above 350 km, the magnetic diffusivity is small, so the magnetic field is mainly controlled by the convection term and is basically frozen in with the plasma. At very low altitude (below 140 km), the plasma flow is nearly zero, so the diffusion term plays the major role. Even though the vertical plasma flow in between 140 and 350 km is quite small, normally less than 100 m/s, it has quite complicated patterns and also slowly changes due to different solar wind forcing. For quiet solar wind conditions (see panel 1b), at high altitude (>300 km altitude), the magnetic pressure gradient and

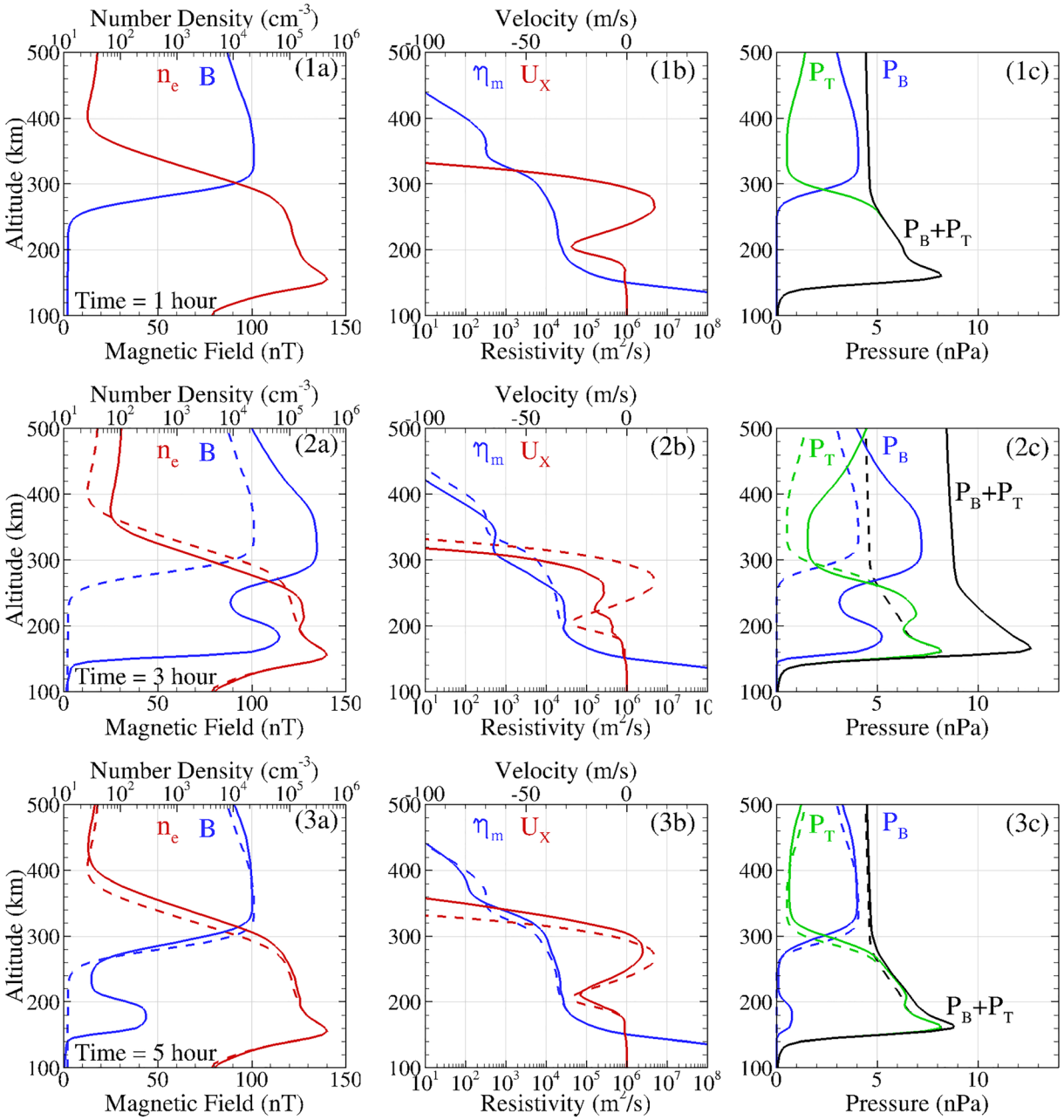

FIGURE 4. Plasma properties in the ionosphere of Venus at 1, 3, and 5 hr. Dashed lines on the second and third rows are results at 1 hr for comparison.

thermal pressure gradient forces are roughly balanced with each other, with a small upward pressure gradient force, so that downward moving solar wind protons are further decelerated. The plasma flow is fully stopped at around 300 km altitude, and planetary plasma between 240 and 300 km altitude is moving upward due to upward pressure gradient force. Below 240 km altitude, downward gravity exceeds the pressure gradient force, which accelerates the plasma downward. This downward flow reaches a local maximum near 200 km altitude, because below the exobase, collisions between ions and neutrals significantly slow down the ion motion. This local peak of the downward plasma flow predicted by our 3D model is quite similar to what was calculated by Cravens et al. (1984) (Figure 1) using a 1D multispecies MHD model. The differences at high altitude are mostly due to the fact that the 1D model imposes an artificial upper boundary (at ~500 km altitude). Also, note that the downward plasma flow

speed can be up to a few km/s near 400 km altitude, much larger than the ~10 m/s used in the upper boundary of the 1D model at 500 km altitude, which could partly explain the density difference from the 1D model and PVO observations (Shinagawa et al., 1987).

The complicated flow patterns basically determine how the magnetic field evolves with time in the subsolar ionosphere. At 3 hr, due to high solar wind pressure, the downward plasma flow is never fully stopped by the ionospheric thermal pressure gradient force, providing continuous downward supply of the magnetic flux from the high altitude. The magnetic field has a local minimum around 240 km altitude, where the downward flow has a local peak. This is because the magnetic fluxes should be conserved, meaning that $V_X B_Y$ should be a constant, and thus a local maximum of $|V_X|$ results in a local minimum of $|B_Y|$. Note that both V_X and B_Y are negative values in the coordinate used. At 5 hr, the plasma condition is fairly similar to 1 hr, except that between 150 and 210 km altitude, there is some remaining magnetic field that was formed during the high-pressure pulse. Simulation results show that at 5 hr (panel 3a), 2 hr after the solar wind returns to normal, the magnetic field in the ionosphere ~200 km altitude is still about 40 nT. It has been suggested by Luhmann et al. (1983) that a large-scale magnetic field could have an effect on the ionosphere and should be included in the ionospheric models. Our results show that those "fossil" magnetic fields in the ionosphere indeed act as an additional obstacle to the solar wind (as shown in panel 3b), help to further slowdown the shocked solar wind, and alter the density and pressure in the ionosphere (see panels 3a and 3c). Model results clearly show that the state of the ionosphere not only depends on the current solar wind condition but is also a complex function of past solar wind conditions, similar to Titan and Mars (Bertucci et al., 2008; Ma et al., 2009, 2014).

4. Discussion and Summary

We performed a time-dependent simulation to examine the response of the near-Venus space to a dynamic pressure (density) enhancement of the solar wind. Simulation results show that the intrinsic time scales for different plasma regions such as the ionosphere and IM are very different. It takes less than ~2 min for the magnetosheath and the IM to respond to solar wind pressure variations, but the response time of the ionosphere is over a much longer time scale of at least hours. The study also shows that the total ion escape rate increases with solar wind dynamic pressure but not linearly due to the long internal response time of the ionosphere.

The simulation results also reveal the controlling processes of the formation and evolution of the large-scale magnetic field in the ionosphere. The large-scale magnetic fields form gradually in the ionosphere during the high-solar wind dynamic pressure period via downward convection of the plasma and associated magnetic flux. After the solar wind pressure drops to below the value of the peak ionospheric thermal pressure, there is no more supply of magnetic flux from above, so the magnetic field gradually decreases through diffusion. In addition, we find that those "fossil" magnetic fields also play important roles in the ionosphere dynamics and can act as additional obstacles to the shocked solar wind plasma. Thus, the state of the ionosphere not only depends on the current solar wind condition but is also a complex function of the past solar wind condition. These large-scale fields may also be twisted to form flux ropes, as suggested by Russell (1990) and will be the subject to future studies. In this study, we have only focused on a particular change in the solar wind, namely, solar wind density pulses. The system response to other types of solar changes (e.g., solar minimum EUV conditions), and solar wind disturbances are also of interest and will be the subject of future studies.

Acknowledgments

This work was supported by NASA's Solar System Working Program. Resources supporting this work were provided by the NASA High-End Computing (HEC) Program through the NASA Advanced Supercomputing (NAS) Division at Ames Research Center. The BATS-RUS code is publicly available from http://csem.engin.umich.edu/tools/swmf. Simulation results can be obtained at https://agudata.epss.ucla.edu/AGUDATA_FROM_CALLISTO/2020_GRL_Venus_pubdata/.

References

Bertucci, C., Achilleos, N., Dougherty, M. K., Modolo, R., Coates, A. J., Szego, K., et al. (2008). The magnetic memory of Titan's ionized atmosphere. *Science*, *321*(5895), 1475–1478. https://doi.org/10.1126/science.1159780

Brace, L. W., Kasprzak, W. T., Taylor, H. A., Theis, R. F., Russell, C. T., Barnes, A., et al. (1987). The ionotail of Venus: Its configuration and evidence for ion escape. *Journal of Geophysical Research*, *92*(A1), 15–26. https://doi.org/10.1029/JA092iA01p00015

Cloutier, P. A. (1984). Formation and dynamics of large-scale magnetic structures in the ionosphere of Venus. *Journal of Geophysical Research*, *89*(A4), 2401–2405. https://doi.org/10.1029/JA089iA04p02401

Cravens, T. E. (1989). The solar wind interaction with non-magnetic bodies and the role of small-scale structures. In J. H. Waite Jr., J. L. Burch, & R. L. Moore (Eds.), *Solar system plasma physics*, *Geophysical Monograph Series* (Vol. 54, pp. 353–366). Washington, DC: American Geophysical Union. https://doi.org/10.1029/GM054p0353

Cravens, T. E., Shinagawa, H., & Nagy, A. F. (1984). The evolution of large-scale magnetic fields in the ionosphere of Venus. *Geophysical Research Letters*, *11*, 267–270. https://doi.org/10.1029/GL011i003p00267

Edberg, N. J. T., Nilsson, H., Futaana, Y., Stenberg, G., Lester, M., Cowley, S. W. H., et al. (2011). Atmospheric erosion of Venus during stormy space weather. *Journal of Geophysical Research*, *116*, A09308. https://doi.org/10.1029/2011JA016749

Elphic, R. C., Russell, C. T., Slavin, J. A., & Brace, L. H. (1980). Observations of the dayside ionopause and ionosphere of Venus. *Journal of Geophysical Research*, *85*(A13), 7679–7696. https://doi.org/10.1029/JA085iA13p07679

Fedorov, A., Barabash, S., Sauvaud, J.-A., Futaana, Y., Zhang, T. L., Lundin, R., & Ferrier, C. (2011). Measurements of the ion escape rates from Venus for solar minimum. *Journal of Geophysical Research*, *116*, A07220. https://doi.org/10.1029/2011JA016427

Futaana, Y., Stenberg Wieser, G., Barabash, S., & Luhmann, J. G. (2017). Solar Wind Interaction and Impact on the Venus Atmosphere. *Space Science Reviews*, *212*, 1453–1509. https://doi.org/10.1007/s11214-017-0362-8

Luhmann, J. G., Elphic, R. C., Russell, C. T., Brace, L. H., & Hartle, R. E. (1983). Effects of large-scale magnetic fields in the Venus ionosphere. *Advances in Space Research*, *2*(10), 17–21.

Luhmann, J. G., Elphic, R. C., Russell, C. T., Mihalov, J. D., & Wolfe, J. H. (1980). Observations of large scale steady magnetic fields in the dayside Venus ionosphere. *Geophysical Research Letters*, *7*(11), 917–920. https://doi.org/10.1029/GL007i011p00917

Luhmann, J. G., Kasprzak, W. T., & Russell, C. T. (2007). Space weather at Venus and its potential consequences for atmosphere evolution. *Journal of Geophysical Research*, *112*, E04S10. https://doi.org/10.1029/2006JE002820

Luhmann, J. G., Russell, C. T., & Elphic, R. C. (1984). Time scales for the decay of induced large-scale magnetic fields in the Venus ionosphere. *Journal of Geophysical Research*, *89*(A1), 362–368. https://doi.org/10.1029/JA089iA01p00362

Ma, Y. J., Fang, X., Nagy, A. F., Russell, C. T., & Toth, G. (2014). Martian ionospheric responses to dynamic pressure enhancements in the solar wind. *Journal of Geophysical Research: Space Physics*, *119*, 1272–1286. https://doi.org/10.1002/2013JA019402

Ma, Y. J., Nagy, A. F., Russell, C. T., Strangeway, R. J., Wei, H. Y., & Toth, G. (2013). A global multispecies single-fluid MHD study of the plasma interaction around Venus. *Journal of Geophysical Research: Space Physics*, *118*, 321–330. https://doi.org/10.1029/2012JA018265

Ma, Y. J., Russell, C. T., Nagy, A. F., Toth, G., Bertucci, C., Dougherty, M. K., et al. (2009). Time-dependent global MHD simulations of Cassini T32 flyby: From magnetosphere to magnetosheath. *Journal of Geophysical Research*, *114*, A03204. https://doi.org/10.1029/2008JA013676

McComas, D. J., Spence, H. E., Russell, C. T., & Saunders, M. A. (1986). The average magnetic field draping and consistent plasma properties of the Venus magnetotail. *Geophysical Research Letters*, *91*(A7), 7939. https://doi.org/10.1029/JA091iA07p07939

Phillips, J. L., & Russell, C. T. (1987). Upper limit on the intrinsic magnetic field of Venus. *Journal of Geophysical Research*, *92*(A3), 2253–2263. https://doi.org/10.1029/JA092iA03p02253

Romanelli, N., DiBraccio, G., Modolo, R., Leblanc, F., Espley, J., Gruesbeck, J., et al. (2019). Recovery timescales of the dayside Martian magnetosphere to IMF variability. *Geophysical Research Letters*, *46*, 10,977–10,986. https://doi.org/10.1029/2019GL084151

Russell, C. (1990). Magnetic flux ropes in the ionosphere of Venus. *Physics of Magnetic Flux Ropes*, *58*, 413–423. https://doi.org/10.1029/GM058p0413

Russell, C. T., Chou, E., Luhmann, J. G., Gazis, P., Brace, L. H., & Hoegy, W. R. (1988). Solar and interplanetary control of the location of the Venus bow shock. *Journal of Geophysical Research*, *93*(A6), 5461–5469. https://doi.org/10.1029/JA093iA06p05461

Russell, C. T., Luhmann, J. G., & Elphic, R. C. (1983). The properties of the low altitude magnetic belt in the Venus ionosphere. *Advances in Space Research*, *2*(10), 13–16.

Shinagawa, H. (1996a). A two-dimensional model of the Venus ionosphere, 1. Unmagnetized ionosphere. *Journal of Geophysical Research*, *101*(A12).

Shinagawa, H. (1996b). A two-dimensional model of the Venus ionosphere: 2. Magnetized ionosphere. *Journal of Geophysical Research*, *101*(A12), 26,921–26,930. https://doi.org/10.1029/96JA01362

Shinagawa, H., & Cravens, T. E. (1988). A one-dimensional multispecies magnetohydrodynamic model of the dayside ionosphere of Venus. *Journal of Geophysical Research*, *93*(A10), 11,263–11,277. https://doi.org/10.1029/JA093iA10p11263

Shinagawa, H., Cravens, T. E., & Nagy, A. F. (1987). A one-dimensional time-dependent model of the magnetized ionosphere of Venus. *Journal of Geophysical Research*, *92*(A7), 7317–7330. https://doi.org/10.1029/JA092iA07p07317

Shinagawa, H., Kim, J., Nagy, A. F., & Cravens, T. E. (1991). A comprehensive magnetohydrodynamic model of the Venus ionosphere. *Journal of Geophysical Research*, *96*(A7), 11,083–11,095. https://doi.org/10.1029/90JA02505

Tóth, G., van der Holst, B., Sokolov, I. V., de Zeeuw, D. L., Gombosi, T. I., Fang, F., et al. (2012). Adaptive numerical algorithms in space weather modeling. *Journal of Computational Physics*, *231*(3), 870–903. https://doi.org/10.1016/j.jcp.2011.02.006

Villarreal, M. N., Russell, C. T., Wei, H. Y., Ma, Y. J., Luhmann, J. G., Strangeway, R. J., & Zhang, T. L. (2015). Characterizing the low-altitude magnetic belt at Venus: Complementary observations from the Pioneer Venus Orbiter and Venus Express. *Journal of Geophysical Research: Space Physics*, *120*, 2232–2240. https://doi.org/10.1002/2014JA020853

Zhang, T.-L., Luhmann, J. G., & Russell, C. T. (1990). The solar cycle dependence of the location and shape of the Venus bow shock. *Journal of Geophysical Research*, *95*(A9), 14,961–14,967. https://doi.org/10.1029/JA095iA09p14961